Available online at www.sciencedirect.com
ScienceDirect
Journal of Solid State Chemistry 181 (2008) 913–919
JOURNAL OF SOLID STATE CHEMISTRY
www.elsevier.com/locate/jssc

Characterization and activity of visible-light-driven TiO_2 photocatalyst codoped with nitrogen and cerium

Chao Liu[a,1], Xinhu Tang[a], Cehui Mo[a,*], Zhimin Qiang[b]

[a]*Department of Environmental Engineering, Jinan University, Guangzhou 510632, China*
[b]*State Key Laboratory of Environmental Aquatic Chemistry, Research Center for Eco-Environmental Sciences, Chinese Academy of Sciences, Beijing 100085, China*

Received 31 October 2007; received in revised form 11 January 2008; accepted 20 January 2008
Available online 4 February 2008

Abstract

Nitrogen and cerium codoped TiO_2 photocatalysts were prepared by a modified sol–gel process with doping precursors of cerium nitrate and urea, and characterized by X-ray diffraction (XRD), thermogravimetry–differential scanning calorimetry (TG–DSC), X-ray photoelectron spectra (XPS) and ultraviolet–visible light diffuse reflectance spectra (UV–vis DRS). Results indicate that anatase TiO_2 is the dominant crystalline type in as-prepared samples, and CeO_2 crystallites appear as the doping ratio of Ce/Ti reaches to 3.0 at%. The TiO_2 starts to transform from amorphous phase to anatase at 987.1 K during calcination, according to the TG–DSC curves. The XPS show that three major metal ions of Ce^{3+}, Ce^{4+}, Ti^{4+} and one minor metal ion of Ti^{3+} coexist on the surface. The codoped TiO_2 exhibits significant absorption within the range of 400–500 nm compared to the non-doped and only nitrogen-doped TiO_2. The enhanced photocatalytic activity of the codoped TiO_2 is demonstrated through degradation of methyl orange under visible light irradiation.

Keywords: TiO_2 photocatalyst; Codoping; Nitrogen; Cerium; Visible light

1. Introduction

TiO_2 is one of the most promising photocatalyst due to its optical and electronic properties, stability, low cost and non-toxicity, and can be applied in eliminating persistent organic pollutants in air or water [1–4]. However, the widespread technological applications of TiO_2 are impaired by its wide band gap (3.2 eV) which requires ultraviolet irradiation (wavelength $\lambda < 387$ nm) for photocatalytic activation [3]. Research efforts have been performed to synthesize specific TiO_2 that can be effectively activated by visible light, the main portion of solar light. It was initially reported that the doping of various transitional metal ions into TiO_2 could shift its optical absorption edge from UV into visible light range, but a prominent change in TiO_2 band gap was not observed [5,6].

Recently, Asahi et al. [7] reported that nitrogen doping could narrow the band gap and hence induce the visible light absorption of TiO_2. Since then, more detailed efforts have been devoted to the investigation of nitrogen doping [1,2,8,9]. It was demonstrated that nitrogen doping extended the optical absorption edge of TiO_2 into visible light region. However, the practical application of the N–TiO_2 is still hindered by its low reactivity and quantum efficiency [3]. Furthermore, the artificially created crystalline lattice lacuna could affect the long-term stability of TiO_2.

To solve these problems, TiO_2 photocatalysts codoped with nitrogen and metal or other non-metal ions are regarded as a promising approach. It was reported that nitrogen and lanthanum codoped TiO_2 nanoparticles showed a superior photocatalytic activity on degradation of methyl orange under visible light irradiation compared to N-doped or La-doped TiO_2 [10,11]. The N–F codoped TiO_2 synthesized through spray pyrolysis technology

*Corresponding author. Fax: +86 20 85226615.
E-mail address: tchmo@jnu.edu.cn (C. Mo).
[1]Present address: State Key Laboratory of Environmental Aquatic Chemistry, Research Center for Eco-Environmental Sciences, Chinese Academy of Sciences, Beijing 100085, China.

0022-4596/$ - see front matter © 2008 Published by Elsevier Inc.
doi:10.1016/j.jssc.2008.01.031

exhibited better photocatalytic activity on degradation of acetaldehyde under both UV and visible light irradiation than Degussa P25, a commercial TiO_2 photocatalyst [3,4]. Besides, Br–Cl [12] codoped TiO_2 was also attempted to enhance the visible light absorption of TiO_2.

Doping TiO_2 with lanthanide element has attracted increasing attention due to their special $4f$ electron configuration [13–22]. Lanthanide ions could form complexes with various Lewis bases in the interaction of the functional groups with their f-orbital, enhancing the photocatalytic activity. Among them, the cerium doping has received much more interest due to following reasons: (1) the redox couple Ce^{3+}/Ce^{4+} makes cerium oxide shift between CeO_2 and Ce_2O_3 under oxidizing and reducing conditions [13,18]; (2) the easy formation of labile oxygen vacancies with the relatively high mobility of bulk oxygen species [13,15]; and (3) different optical and photocatalytic properties caused by different ions (Ce^{3+}/Ce^{4+}) [14]. Taking account of these features, it could be expected to fabricate an enhanced visible-light-driven photocatalyst by introducing cerium into N–TiO_2 particles. In this study a series of visible-light-driven TiO_2 photocatalyst codoped with nitrogen and cerium were synthesized and characterized, and their photocatalytic activities were examined through degradation of methyl orange under visible light irradiation.

2. Experimental details

2.1. Preparation

N–Ce codoped nano-TiO_2 photocatalysts were synthesized by a modified sol–gel process. Briefly, a varied amount of $Ce(NO_3)_3$ together with a constant amount of urea (atomic ratio of urea to tetrabutyl titanate = 0.5) were dissolved in anhydrous ethanol according to the doping ratio of Ce/Ti of 0, 0.1, 0.3, 1.0, 3.0 and 10.0 at%, respectively. The resulting solution was added dropwise into a tetrabutyl titanate solution with anhydrous ethanol as solvent at room temperature under vigorously stirring condition to carry out hydrolysis. The mixture was stirred continuously until the formation of gel, which was then dried at 383 K for 8 h in air. The resulting powders were finally calcined at 773 K for 2 h to be crystallized. For comparison, the as-prepared photocatalysts were denoted as N–xCe–TiO_2, where x represented the nominal atomic ratio of cerium to titanium.

2.2. Characterization

To determine the crystalline structure of the prepared TiO_2, X-ray diffraction (XRD) patterns were recorded on an XD-2 diffractometer (Microstructure Analytical Laboratory, Peking University, China). Cu$K\alpha$ radiation mode was used over the 2θ range of 20–80° at a scanning rate of $8^\circ\,min^{-1}$. The accelerating voltage and emission current were applied at 36 kV and 20 mA, respectively. Thermogravimetry–differential scanning calorimetry (TG–DSC) was analyzed in α-Al_2O_3 pans with a NETZSHC STA449C thermal analysis system under nitrogen gas flow from 293 to 1273 K at a heating rate of $20\,K\,min^{-1}$. To obtain the chemical composition and chemicals state information, X-ray photoelectron spectra (XPS) were collected with a PHI Quantum ESCA microprobe system, using the Al$K\alpha$ X-ray with the energy of 1486.6 eV and the working pressure of less than 5×10^{-7} Pa. The ultraviolet–visible light diffuse reflectance spectra (UV–vis DRS) of the prepared TiO_2 were measured with a Hitachi U3010 spectrophotometer at room temperature in the wavelength range of 240–800 nm using $BaSO_4$ as reference.

2.3. Photocatalytic activity

The photocatalytic activity of the prepared TiO_2 was evaluated through degradation of $10\,mg\,L^{-1}$ methyl orange in an SGY-1 multifunctional photochemical reactor (Nanjing Stonetech Electric Equipment Company, Nanjing, China). The volume of the reaction solution was 50 mL, into which 20 mg of photocatalyst was added. Irradiation was provided by a medium-pressure Hg lamp (300 W) equipped with a cutoff filter to completely remove any radiation below 400 nm and to ensure illumination by visible light only. Sampling was performed at regular time during reaction. The residue concentration of methyl orange was determined by measuring its absorbance at 460 nm using an S54 UV–vis spectrophotometer (Shanghai Lengguang Technology Co. Ltd., Shanghai, China).

3. Results and discussion

3.1. Crystalline structure

The XRD patterns of different N–Ce codoped TiO_2 photocatalysts were given in Fig. 1. It showed that the crystalline structure of the prepared TiO_2 was anatase. Peak B started to appear at the Ce/Ti doping ratio of 3.0 at%. As the Ce/Ti doping ratio increased to 10.0 at%, the peak intensity got strong and could be clearly observed. If peak B came from titanium oxide, it should appear in all patterns. However, it did not follow the obtained results, so it should be ascribed to cerium oxide rather than titanium oxide. According to the diffraction angle of Peak B, it was confirmed to be relevant to CeO_2 [16–20], implying a significant portion of Ce^{3+} ions were oxidized into Ce^{4+} during heating treatment.

The average crystal size can be estimated by the Scherrer's formula, $D=(K\lambda)/(\beta\cos\theta)$, from the integral width of XRD peaks, where K is the Scherrer constant ($K=0.9$), λ is the wavelength of XRD ($\lambda=0.15418$ nm), and β is the full-width at half-maximum (FWHM) of the 1 0 1 plane (in radians) [23]. The crystalline structure and crystal size of the prepared TiO_2 were summarized in Table 1. It is observed that increasing Ce/Ti doping ratio reduced the crystal size. Because the ionic radii of Ce^{3+}

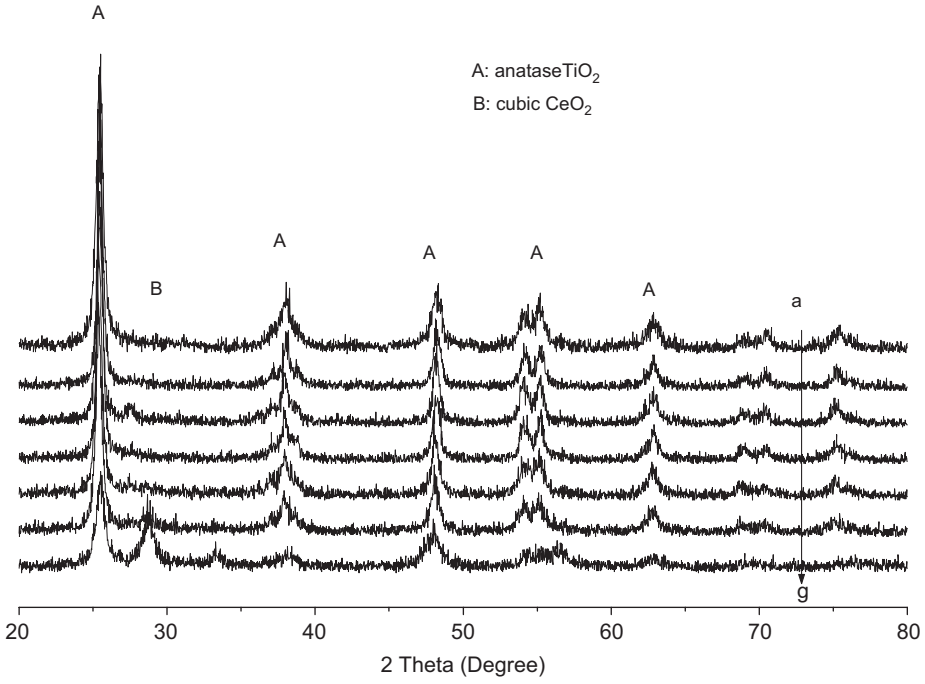

Fig. 1. XRD patterns of prepared TiO_2 photocatalysts: (a) TiO_2; (b) N–TiO_2; (c–g) N–xCe–TiO_2, $x = 0.1\%$, 0.3%, 1.0%, 3.0% and 10.0%.

Table 1
Crystalline properties of prepared TiO_2 photocatalysts

Nanophotocatalyst	Crystalline structure	Crystal size (nm)
TiO_2	Anatase TiO_2	14.0
N–TiO_2	Anatase TiO_2	16.7
N–0.1% Ce–TiO_2	Anatase TiO_2	16.2
N–0.3% Ce–TiO_2	Anatase TiO_2	15.5
N–1% Ce–TiO_2	Anatase TiO_2	15.3
N–3% Ce–TiO_2	Anatase TiO_2, Cubic CeO_2	15.3
N–10% Ce–TiO_2	Anatase TiO_2, Cubic CeO_2	14.1

and Ce^{4+} (0.103 and 0.092 nm, respectively) [24] are much bigger than that of Ti^{4+} (0.065 nm) [25], it is difficult for Ce^{3+} and Ce^{4+} to enter the crystalline lattice of TiO_2 to replace Ti^{4+}. The Ce^{3+} and Ce^{4+} ions seem more likely to complex with the surface oxygen of TiO_2, which suppresses the growth of TiO_2 crystallite [20,21].

3.2. TG–DSC analysis

The TG–DSC of the prepared TiO_2, exemplified by N–10% Ce–TiO_2, was shown in Fig. 2. Results indicated that an endothermic valley (Valley A) appeared at 372.3 K on the DSC curve, and there was 6% weight loss on the TG curve correspondingly due to the evaporation of adsorbed water. As the calcination temperature increased, an exothermic peak (Peak B1) emerged at 542.7 K on the DSC curve. There was about 29% weight loss on the TG curve correspondingly, mainly due to combustion and desorption of organic materials. The exothermic peak

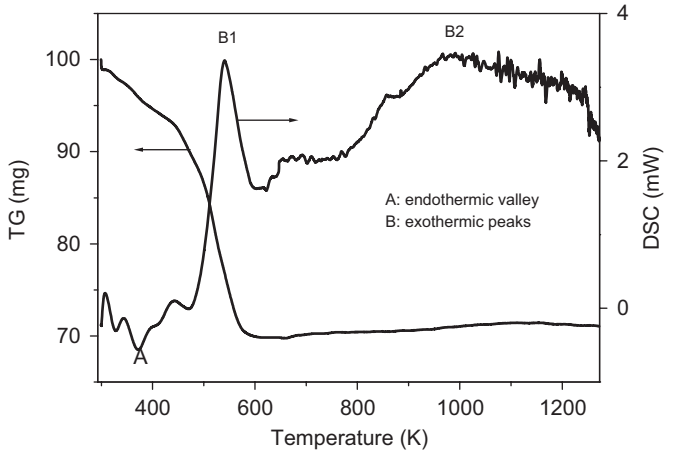

Fig. 2. TG–DSC of N–10% Ce–TiO_2.

(Peak B2) at 987.1 K on the DSC curve implies the phase transformation of TiO_2 from amorphous to anatase, and Peak B2 is very wide, indicating that this phase transformation is quite slow. The cumulative weight loss was approximately 35% at the calcination temperature of 1273 K.

In the whole region of calcination from 300 to 1273 K, the exothermic peak denoting phase transformation from anatase to rutile TiO_2 was not observed. It may imply that N–Ce doping inhibits the phase formation of rutile TiO_2, and it may be mainly attributed to cerium doping. Reddy et al. [16] observed that the CeO_2–TiO_2 mixed oxide with 1:1 molar ratio did not display the rutile phase even up to a calcination temperature of 1073 K, and other results also

showed the stabilization of TiO_2 anatase in cerium doped TiO_2 [17–19]. Due to the bigger ionic radius of Ce^{4+}, it cannot substitute for Ti^{4+} and cerium hence surround the anatase crystallite, forming Ti–O–Ce bonds at the CeO_2–TiO_2 interface. At the interface, Ti^{4+} is expected to substitute for Ce^{4+} in the lattice of the cerium oxide to form octahedral Ti sites. The interaction between the tetrahedral Ti and octahedral Ti could inhibit the anatase to rutile phase transformation [16–18].

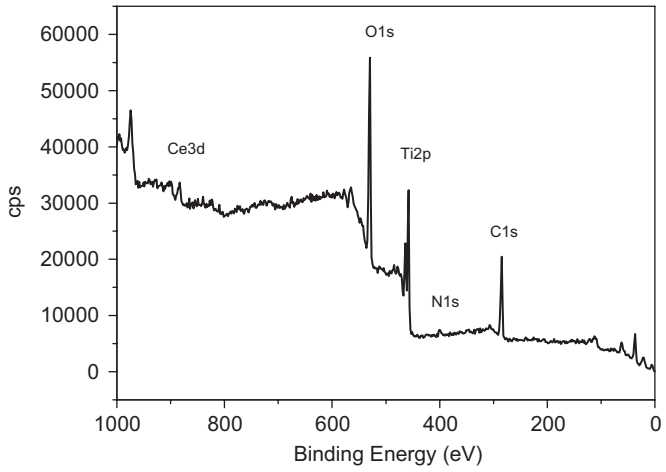

Fig. 3. XPS of N–10% Ce–TiO_2.

3.3. XPS analysis

The N–10% Ce–TiO_2 was further analyzed by XPS to determine the main elements and chemicals state on the TiO_2 surface. The XPS spectrum was shown in Fig. 3. Results indicated that five elements, namely, Ti, O, N, Ce and C, were present together on the TiO_2 surface. N and Ce came from the doping solution, and C probably originated from the calcination residue of organic materials [22]. Fig. 4 showed the high-resolution XPS of N 1*s*, O 1*s*, Ti 2*p* and Ce 3*d* of the N–10% Ce–TiO_2 photocatalyst. The XPS fitting data, including chemical state, binding energy, FWHM and peak area, were summarized in Table 2.

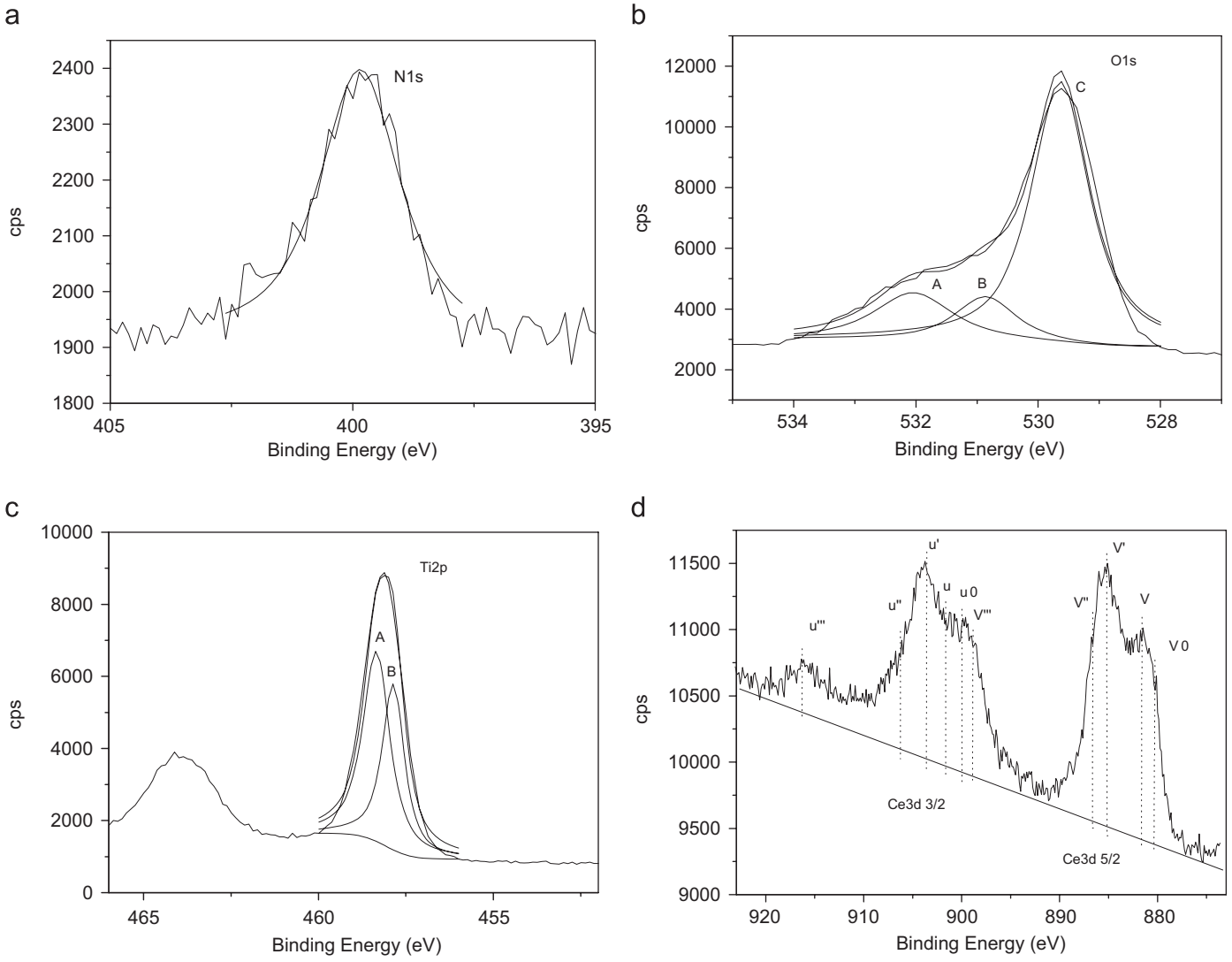

Fig. 4. High-resolution XPS of N–10%Ce–TiO_2: (a) N 1*s*; (b) O 1*s*; (c) Ti 2*p*; and (d) Ce 3*d*.

Table 2
XPS fitting data of N–10% Ce–TiO_2

Element	Chemical state	BE[a] (eV)	FWHM[b] (eV)	Peak area (%)
O1*s*	Crystalline	529.64	1.13	70.33
	Adsorptive	530.86	1.19	12.62
	OH group	532.04	1.53	17.05
N1*s*	Ion	399.85	2.02	100.00
Ti 2*p* 3/2	Ti^{3+}	457.86	0.76	41.85
	Ti^{4+}	458.35	0.92	58.15

[a]BE: binding energy.
[b]FWHM: full-width at half-maximum of peaks.

The substituting N was reported to be responsible for the enhanced visible light absorption based on both theoretical calculation and experimental results [7]. However, Diwald et al. [2] prepared a TiO_2 photocatalyst by heat treatment under NH_3 gas flow, and ascribed the enhanced visible light absorption to a 399.6 eV peak rather than a 396 eV peak that also appeared in XPS. In this case, a small N peak appeared at 399.8 eV, but there was no peak detected at 396 eV (see Fig. 4a). The N peak at 399.8 eV probably reflects a chemical structure like O–Ti–N. In addition, the substituting N atoms may occupy the interstitial sites of the prepared TiO_2 [2,9].

A prominent peak (Peak C) was observed at 529.64 eV (see Fig. 4b), agreeing with the O 1*s* electron binding energy of TiO_2 and CeO_2. There were two other peaks nearby: one at 530.86 eV (Peak B) representing the surface-adsorbed O atoms, and the other at 532.04 eV (Peak A) representing the hydroxyl O atoms [22].

The Ti 2*p* 3/2 peak at 458.35 eV (Peak A) corresponded to Ti^{4+} (see Fig. 4c). Because of the Ce doping, the resulting charge imbalance caused the reduction of Ti^{4+} to Ti^{3+} [13]. The Ti^{3+} peak was found at 457.86 eV (Peak B).

The XPS of Ce 3*d* is quite complicated due to the hybridization of Ce 4*f* and O 2*p* electrons [26], as shown in Fig. 4d. Since Burroughs [27] made his first attempt, much effort has been made to interpret these peaks qualitatively or quantitatively [16,23,28–32]. It was reported that the Ce 3*d* spectra could be assigned to two sets of spin–orbital multiplets, i.e., 3*d* 5/2 and 3*d* 3/2 [16,32] which are denoted as v and u in Fig. 4d, respectively. The peaks denoted as v, v″ and v‴ were attributed to CeO_2 with v and v″ representing a mixed configuration of $(5d\ 6s)^0\ 4f^2$ O $2p^4$ and $(5d\ 6s)^0\ 4f^1$ O $2p^5$, and v‴ representing a pure configuration of $(5d\ 6s)^0\ 4f^0$ O $2p^6$. Meanwhile, v_0 and v′ were attributed to a mixed configuration of $(5d\ 6s)^0\ 4f^2$ O $2p^4$ and $(5d\ 6s)^0\ 4f^1$ O $2p^5$ in Ce_2O_3. Similar assignments could be applied to the *u* class peaks, which corresponded to the Ce 3*d* 3/2 electronic levels. Additionally, many peaks were observed in the Ce 3*d* spectra, indicating the coexistence of Ce^{3+} and Ce^{4+}. However, the diffraction peaks of Ce^{3+} were not observed in Fig. 1. This probably indicated that the Ce^{3+} compound was either amorphous or had a very low content.

3.4. UV–vis DRS

The UV–vis DRS of different N–Ce codoped TiO_2 photocatalysts were shown in Fig. 5. Results indicated that the optical absorption edge was obviously shifted to the visible light range with increasing the Ce/Ti doping ratio. The N–Ce codoped TiO_2 showed a significant absorption from 400 to 500 nm in comparison with the non-doped and N-doped TiO_2. The maximum absorption of visible light was observed for N–10% Ce–TiO_2.

Kubelka–Munk function was used to estimate the band gap energy of the prepared TiO_2 [33] by plotting $[F(R)E]^{1/2}$ versus energy of light (see Fig. 6). The optical absorption threshold (λ_g) was calculated using the equation, $\lambda_g = 1240/E_B$, where E_B is the band gap energy. The values of band gap and absorption band were shown in Table 3. Results indicated that the band gap energies of the N–Ce codoped TiO_2 were between 2.6 and 2.3 eV, considerably narrower than that of non-doped (3.2 eV) or N-doped TiO_2 (2.8 eV). Accordingly, the absorption band of the N–Ce

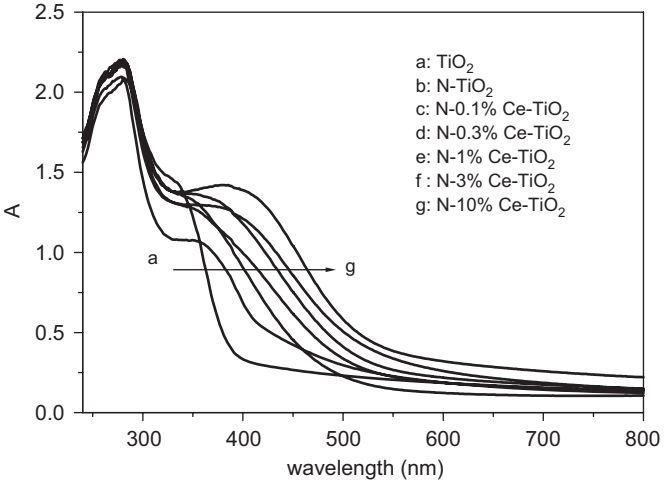

Fig. 5. UV–vis DRS of prepared TiO_2 photocatalysts.

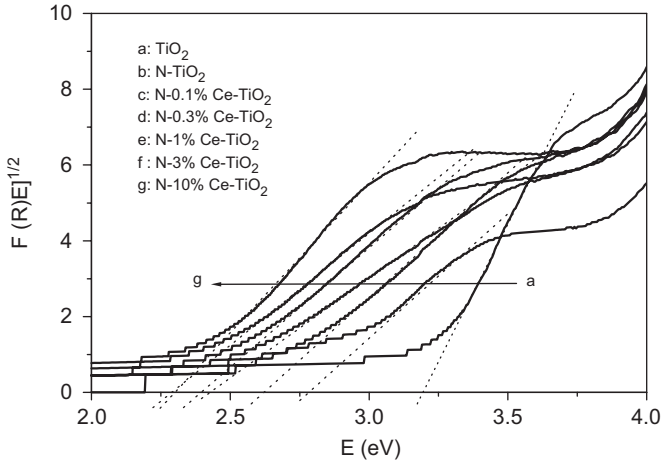

Fig. 6. Plot of Kubelka–Munk function $[F(R)E]^{1/2}$ versus energy of light (E) for prepared TiO_2 photocatalysts.

Table 3
Optical properties of prepared TiO_2 photocatalysts

Nanophotocatalyst	Band gap energy (eV)	Absorption edge wavelength (nm)
TiO_2	3.2	387
N–TiO_2	2.8	443
N–0.1% Ce–TiO_2	2.6	477
N–0.3% Ce–TiO_2	2.4	517
N–1% Ce–TiO_2	2.4	528
N–3% Ce–TiO_2	2.3	535
N–10% Ce–TiO_2	2.3	539

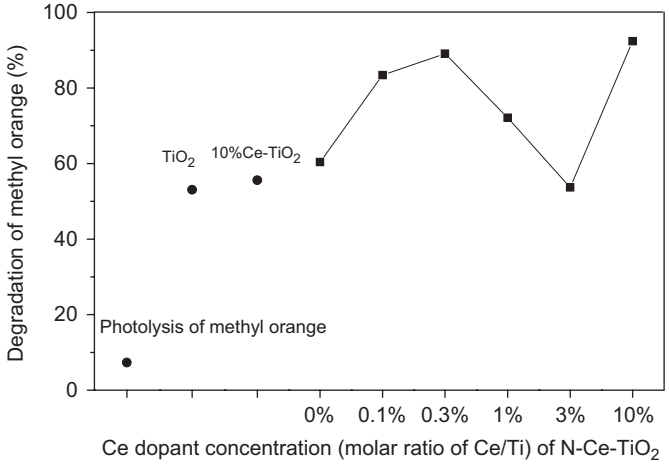

Fig. 7. Degradation of methyl orange with nitrogen and different cerium dopant concentration codoped TiO_2 photocatalysts under visible light irradiation after 2 h.

codoped TiO_2 exhibited a red shift to the visible light range of 477−539 nm in comparison with the non-doped (387 nm) and N-doped TiO_2 (443 nm). It is demonstrated that N–Ce codoped TiO_2 can greatly improve the absorption of visible light. The enhanced visible light absorption may result from: (1) N atoms replace a portion of O atoms in TiO_2 crystallite, forming a new energy level on top of the valence band to generate a red shift [7]; and (2) The specific 4*f* electronic configuration of cerium plays a crucial role in generating electron–hole pairs to improve the visible light response [13].

3.5. Photocatalytic activity

The prepared TiO_2 photocatalysts were used to degrade methyl orange under visible light irradiation for 2 h, and the results were presented in Fig. 7. Results showed that the concentration of methyl orange only decreased 7.3% after 2 h visible light irradiation but without TiO_2. It indicates that the self-sensitization factor of methyl orange was weak effect during the photocatalytic reaction and it could be negligible to evaluate the visible light activity [34]. The codoped TiO_2 (except N–3% Ce–TiO_2) exhibited a higher photocatalytic activity than the non-doped or monodoped TiO_2, indicating that the N–Ce codoping was effective in enhancing visible light response. In this study, the plain TiO_2 photocatalyst exhibits a significant removal of methyl orange. Actually, non-doped titania do not have visible light activity, it may be ascribed to adsorption of reactant and slight dye self-sensitization. Therefore, the actual degradation efficiency will be calculated considering these factors.

The improved photocatalytic activity can be attributed to the co-effect of nitrogen and cerium in TiO_2 powder. Nitrogen doping narrows the band gap of TiO_2 to enhance visible light absorption [4,7]. Cerium doping serves as an electron trap in the reaction because of its varied valences and special 4*f* level [13], as illustrated by the following equations:

$$Ce^{4+} + e^- \rightarrow Ce^{3+} \quad (1)$$

$$Ce^{3+} + O_2 \rightarrow O_2^- + Ce^{4+} \quad (2)$$

$$O_2^{\bullet -} + 2H^+ \rightarrow 2^{\bullet}OH \quad (3)$$

Cerium doping also increases the surface area of TiO_2 by decreasing the crystal size. In addition, the hydroxyl O on TiO_2 surface may prevent the recombination of electrons and holes [16].

The concentration of cerium dopant in N–Ce–TiO_2 photocatalysts directly affects the visible light activity. It might vary from low Ce/Ti atomic ratio range ($\leqslant$1%) to high Ce/Ti ratio range (>1%), which could be similar as Fe-doping [5]. In the low Ce/Ti atomic ratio range there was only one phase (anatase TiO_2) in N–Ce–TiO_2 photocatalysts, and the relationship between cerium content and activity obeyed general transition metal ions doping mechanisms [5,6,13]. As the Ce/Ti doping ratio increased from 0 to 0.3 at%, the dominant Ce^{4+} captured electrons to achieve a higher photocatalytic activity. However, if the Ce/Ti doping ratio continued to increase from 0.3 to 1.0 at%, extra resulting Ce^{3+} ions could introduce the indirect recombination of electrons and holes to reduce the photocatalytic activity, leading to a huge activity decline. Heavily loaded samples are completely different since the phase (cubic CeO_2) other than anatase TiO_2 is present. As the Ce/Ti doping ratio increased from 3.0 to 10.0 at%, a significant content of CeO_2 crystallite was formed on the TiO_2 surface and a ternary oxide, $CeTiO_4$ or $CeTi_2O_6$ crystallite appeared in some measure, which might enhance the visible light absorption and thus improve the photocatalytic activity [35].

4. Conclusions

This study was to prepare and characterize the TiO_2 photocatalysts codoped with nitrogen and cerium. Results indicate that the dominant crystal type of prepared TiO_2 is anatase, and cubic CeO_2 appeared at 3.0 at% of Ce/Ti doping ratio. The XPS analysis indicates that the N–10%Ce–TiO_2 photocatalyst mainly consisted of Ce^{3+},

Ce^{4+}, Ti^{4+} (major ions) and Ti^{3+} (minor ion). The N–Ce codoping could narrow the band gap of TiO_2 photocatalysts, shift the optical threshold to the range of 477–539 nm, and hence lead to a stronger visible light response than N-doped or non-doped TiO_2. The N–Ce codoped TiO_2 exhibited, in general, an enhanced photocatalytic activity on degradation of methyl orange under visible light irradiation in comparison with non-doped or monodoped TiO_2.

Acknowledgments

The authors would like to acknowledge the financial support from National Natural Science Foundation of China (No. 30471007) and Key Scientific Research Project of Ministry of Education of China (No. 02112). The authors also thank Mr. Shuiju Wang at Xiamen University for XPS measurements and analyses and the graduate student Qiaojun Wang at Jinan University for his assistance on experimental work.

References

[1] C. Burda, Y. Lou, X. Chen, A.C.S. Samia, J. Stot, J.L. Gole, Nano Lett. 3 (2003) 1049–1051.
[2] O. Diwald, T.L. Thompson, T. Zubkov, E.G. Goralski, S.D. Walck, J.T. Yates, J. Phys. Chem. B 108 (2004) 6004–6008.
[3] D. Li, H. Haneda, S. Hishata, N. Ohashi, Chem. Mater. 17 (2005) 2588–2595.
[4] D. Li, H. Haneda, S. Hishata, N. Ohashi, Chem. Mater. 17 (2005) 2596–2602.
[5] M.I. Litter, J.A. Navío, J. Photochem. Photobiol. A 98 (1996) 171–181.
[6] J.C.S. Wu, C.H. Chen, J. Photochem. Photobiol. A 163 (2004) 509–515.
[7] R. Asahi, T. Morikawa, T. Ohwaki, K. Aoki, Y. Taga, Science 293 (2001) 269–271.
[8] X. Chen, C. Burda, J. Phys. Chem. B. 108 (2004) 15446–15449.
[9] E. Gyorgy, A. Perez del pino, P. Serra, J.L. Morenza, Surf. Coat Technol. 173 (2003) 265–270.
[10] H. Wei, W. Wu, N. Lun, F. Zhao, J. Mater. Sci. 39 (2004) 1305–1308.
[11] Y. Sakatani, J. Nunoshige, H. Ando, K. Okusako, H. Koike, T. Takata, J.N. Kondo, M. Hara, K. Domen, Chem. Lett. 32 (2003) 1156–1157.
[12] H. Luo, T. Takata, Y. Lee, J. Zhao, K. Domen, Y. Yan, Chem. Mater. 16 (2005) 846–849.
[13] F.B. Li, X.Z. Li, M.F. Hou, K.W. Cheah, W.C.H. Choy, Appl. Catal. A: Gen. 285 (2005) 181–189.
[14] J.M. Coronado, A.J. Maira, A. Martinez-Arias, J.C. Conesa, J. Soria, J. Photochem. Photobiol. A 150 (2002) 213–221.
[15] B.M. Reddy, P.M. Sreekanth, E.P. Reddy, Y. Yamada, Q. Xu, H. Sakurai, T. Kobayashi, J. Phys. Chem. B 106 (2002) 5695–5700.
[16] B.M. Reddy, A. Khan, Y. Yamada, T. Kobayashi, S. Loridant, J. Volta, J. Phys. Chem. B. 107 (2003) 5162–5167.
[17] J. Lin, J.C. Yu, J. Photochem. Photobiol. A 116 (1998) 63–67.
[18] J. Fang, X. Bi, D. Si, Z. Jiang, W. Huang, Appl. Surf. Sci. 253 (2007) 8952–8961.
[19] T. López, F. Rojas, R. Alexander-katz, F. Galindo, A. Balankin, A. Buljan, J. Solid State Chem. 177 (2004) 1873–1885.
[20] Z. Liu, B. Guo, L. Hong, H. Jiang, J. Phys. Chem. Solids 66 (2005) 161–167.
[21] Y. Xie, C. Yuan, Appl. Catal. B: Environ. 46 (2003) 251–259.
[22] F.B. Li, X.Z. Li, M.F. Hou, Appl. Catal. B: Environ. 48 (2004) 185–194.
[23] P.W. Park, J.S. Ledford, Langmuir 12 (1996) 1794–1799.
[24] 〈http://www.webelements.com/webelements/elements/text/Ce/radii.html〉.
[25] 〈http://www.webelements.com/webelements/elements/text/Ti/radii.htmlE-Host〉.
[26] F. Bozon-Verduraz, A. Bensalem, M. Delamar, G. Bugli, Appl. Catal. A: Gen. 121 (1995) 81–93.
[27] P. Burroughs, A. Hamnett, A.F. Orchard, G. Thornton, J. Chem. Soc. Dalton Trans. 17 (1976) 1686–1698.
[28] M.S.P. Francisco, V.R. Mastelaro, P.A.P. Nascente, A.O. Florentino, J. Phys. Chem. B. 105 (2001) 10515–10522.
[29] J. Rynkowski, J. Farbotko, R. Touroude, L. Hilaire, Appl. Catal. A: Gen. 203 (2000) 335–348.
[30] B.M. Reddy, A. Khan, Y. Yamada, T. Kobayashi, S. Loridant, J. Volta, Langmuir 19 (2003) 3025–3030.
[31] F. Larachi, J. Pierre, A. Adnot, A. Bernis, Appl. Surf. Sci. 195 (2002) 236–250.
[32] J. Silvestre-Albero, F. Rodríguez-Reinoso, A. Sepúlveda-Escribano, J. Catal. 210 (2002) 127–136.
[33] W. Zhao, W. Ma, C. Chen, J. Zhao, Z. Shuai, J. Am. Chem. Soc. 126 (2004) 4782–4783.
[34] S. Al-Qaradawi, S.R. Salman, J. Photochem. Photobiol. A 148 (2002) 161–168.
[35] S. Otsuka-Yao-Matsuo, T. Omata, M. Yoshimura, J. Alloys Compd. 376 (2004) 262–267.